Journal of Energy Storage 68 (2023) 107580

Contents lists available at ScienceDirect

Journal of Energy Storage

journal homepage: www.elsevier.com/locate/est

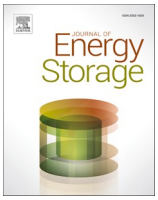

Research Paper

Optimized cooling and thermal analysis of lithium-ion pouch cell under fast charging cycles for electric vehicles

Ayodeji Adeniran , Sam Park *

Department of Mechanical Engineering, University of Louisville, 2301 S 3rd St, Louisville, KY 40292, United States of America

ARTICLE INFO

Keywords:
Battery Thermal Management
Lithium-ion battery
Liquid cooling
Thermal modeling

ABSTRACT

This study used a multidomain modeling approach to perform a thermal analysis of commercial 65 Ah pouch-type batteries configured in a 1P4S configuration (1 parallel and 4 series battery). The study aimed to analyze the thermal behavior of four different cooling configurations, namely single cell with ambient cooling, 1P4S with ambient cooling, 1P4S with only bottom liquid cooling, and 1P4S with two-side liquid cooling. The Newman, Tiedemann, Gu, and Kim (NTGK) model was used for the subscale electrochemical modeling, while Computational Fluid Dynamics (CFD) was used to analyze the thermal behavior during different fast charging rates that are commonly used for electric vehicles. The results of the study showed that using two cooling plates with opposing flow directions instead of one-side cooling reduced the maximum temperature difference by 50 % from 10 °C to 5 °C and reduced the maximum temperature by 7 °C during charging at 1.98C. This suggests that the use of two-side liquid cooling can significantly improve the thermal performance of the battery, which is essential for fast charging and overall battery performance. The implications of this study for the industry are significant, as it provides insight into how to improve the design and thermal management of battery packs for electric vehicles. By using multidomain modeling and CFD analysis, battery manufacturers can optimize the design of their battery packs to improve thermal management, reduce the risk of thermal runaway, and improve battery performance and longevity. This can lead to the development of more reliable and efficient electric vehicles, which can help to accelerate the adoption of electric vehicles worldwide.

1. Introduction

Lithium-ion batteries have become ubiquitous in the automotive industry due to their superior advantages over other battery types, such as high energy density, low self-discharge rate, lightweight, zero memory effect, and long life cycle [1,2]. However, lithium batteries work optimally within a narrow temperature range: of 15–40 °C [3–5]. At a temperature lower than this range ionic conductivity in the electrolyte is significantly reduced which leads to lower power output, lithium plating, and subsequent degradation of the battery, while at higher temperatures accelerated exothermic reaction leads to corrosion of battery materials, overall cell degradation, and results in a thermal runaway at temperatures above 80 °C [3]. In addition to keeping the temperature within a narrow operating range, it is also important to keep the maximum temperature difference within the battery cell or module low; a value of <5 °C is the recommended maximum temperature difference within a cell [6].

The majority of current research works into battery cooling design and optimization have been focused on cylindrical and prismatic type cells. Recently pouch-type cells have become of interest due to their higher energy density than cylindrical cells [7]. Presently, various thermal management systems have been proposed for cooling lithium-ion batteries: air cooling [8,9], indirect liquid cooling [10,11], direct liquid or immersion cooling [4,12], passive cooling using phase change materials [13,14], heat pipes [15], and hybrid methods involving a combination of two or more these approaches [16]. However, in terms of commercial application in electric vehicles, only air [17] and liquid cooling have been implemented on a large scale, while the others are still in the research phase. Liquid cooling is still the most efficient and researched system so far due to its high thermal capacity; as a result, the current research trend is to find ways of improving the designs of the liquid-cooled cold plates to achieve better and more cost-effective thermal control.

Typically, all commercial implementations of liquid cooling systems for batteries have focused on indirect cooling arrangement using a cold plate heat exchanger. Patil et al. [18] investigated a U-turn-shaped

* Corresponding author.
E-mail address: sam.park@louisville.edu (S. Park).

https://doi.org/10.1016/j.est.2023.107580
Received 27 May 2022; Received in revised form 1 April 2023; Accepted 28 April 2023
Available online 19 May 2023

narrow hexagonal channel cold plate for the thermal management of a 20 Ah lithium-ion pouch cell and optimized the cooling performance by varying the geometry and flow parameters. They investigated the sensitivity of the battery to factors such as inlet coolant temperature, volume flow rate, number of channels, and maximum channel width. Meanwhile, Huo et al. [19] investigated thermal management using a mini-channel cold plate for prismatic type cells with varying numbers of channels, flow direction, inlet mass flow rate, and ambient temperature during a discharge process. It was shown that increasing the mass flow rate yields better cooling performance, but an upper limit exists beyond which the system efficiency decreases. Monika et al. [20] proposed the utilization of the Tesla valve to replace the conventional rectangular micro-channels in cold plate applications to reduce local temperature distribution in the battery cells. It was shown that the heat transfer was enhanced mainly due to flow bifurcation and mixing with a significant pressure reduction. Their analyses showed the cold plate with 4 channels and 8.82 mm valve distance had the greatest effect at reducing the cells temperature difference.

Hunt et al. [10] experimented to explore the effect of cell surface cooling and cell tab cooling on 5 Ah Lithium-ion pouch cells. They found that at a high discharge rate, surface cooling led to a loss of usable capacity three times higher than tab cooling due to the high-temperature difference in the internal layers of the pouch cell, whereas tab cooling did not cause such a high temperature disparity. Sheng et al. [21] carried out a numerical analysis of a serpentine-channeled cold plate with two inlets and two outlets. Their results showed that increasing the channel width has a strong impact on the cooling power consumption but a weak impact on cell temperature rise. Kong et al. [22] proposed a new cold plate using divergent-shaped channels which showed higher heat dissipation capacity and lower frictional resistance compared to the conventional straight channeled cold plate. The increased cross-sectional area in their design reduced the coolant pressure drop by 7.2 % and cell maximum temperature by 0.80 K compared to a straight-channel cold plate. Kalkan et al. [23] proposed cooling a lithium-phosphate battery subjected to 1C - 5C discharge rates using mini-channel cold plate designs which were investigated experimentally alongside a serpentine-channel cold plate. Their experimental results showed that the maximum surface temperature of the cell was reduced by 5.7 °C and the surface temperature distribution of the cell was improved by 40 % compared to the serpentine channel plate. Zhang et.al [24] carried out a numerical study of the performance of straight channels cold plate and inclined channels cold plate under different coolants, channel numbers and mass flow rates. Their results showed that heat transfer performance of the inclined channels was much better than straight channels and the performance improves as the inclined angle increases.

To reduce the cost of experimental procedures and more quickly design a working battery heat exchanger, accurate thermal modeling of lithium-ion battery cells/packs is needed for efficient thermal control of the battery system. However, such modeling is difficult to implement due to the multidomain and multiscale nature of the Li-ion battery. The multi-scale multi-domain (MSMD) [25] approach simplifies the battery modeling complexity by efficiently coupling electrochemical and thermal physics across the different battery length scales [26]. Several empirical sub-models exist in the literature to implement the MSMD with the most popular being: Newman, Tiedemann, Gu, and Kim's (NTGK) model [27], the equivalent circuit (ECM) model [28], and Newman's Pseudo-two-dimensional (P2D) model [29]. These models enhance the easy prediction of thermal responses in battery packs and have been integrated into several battery modeling applications including ANSYS Fluent and COMSOL Multiphysics. Zhang et al. [29] used the NTGK model in ANSYS Fluent to analyze the thermal characteristics of a 20-Ah prismatic-type 6s4p lithium-ion battery cooled by cold plates placed between adjacent cells. They investigated the effects of inlet water velocity and inlet water temperature under a 5C cell discharge rate, with and without an external shorting condition. Their result shows that at a coolant inlet velocity of 2 $m{\cdot}s^{-1}$, the maximum temperature was below 40 °C and the temperature difference was below 5 °C.

Most of the studies on pouch cells presented in this introduction have focused on using cooling plates sandwiched between layers of pouch cells; however, this would substantially increase the weight and volume of the entire battery pack for large format pouch cells. Additionally, the sizes of pouch cells examined in previous studies were not of practical size for use in an electric vehicle. Furthermore, none of these studies explored the combined effect of the interaction between ambient temperature, charging time, and coolant temperature on the peak temperature and thermal gradients in the module. In this study, we took the analysis of battery cooling a step further by carrying out a detailed thermal analysis of one-sided and two-sided liquid cooling of an electric vehicle battery module under different cell charging/discharging rates, coolant, and ambient temperatures using a multi-domain simulation approach. Analysis was performed using nine unique charging profiles which are characteristic of electric vehicle operations.

Nomenclature

a	area of the electrode sandwich sheet [m^2]
A_c	cross-sectional area [m^2]
C_p	specific heat capacity [J Kg^{-1} K^{-1}]
J	Joule
D_h	hydraulic diameter [m]
h	heat transfer coefficient [W• $(m^2K)^{-1}$]
k	thermal conductivity [W• $(mK)^{-1}$]
P	pressure [Pa]
Q	battery capacity (Ah)
$\dot{Q}$	heat generation rate of the battery[$W{\cdot}m^{-3}$]
T	temperature [K]
V	fluid's inlet velocity [$m{\cdot}s^{-1}$]
Vol	volume of the battery cell [m^3]
j	current transfer rate [$A{\cdot}m^{-3}$]

Subscripts

max	maximum
min	minimum
ECh	electrochemical
ohm	ohmic
ref	reference

Greek

δ	thickness [m]
σ	electric conductivity [Ω·m]
μ	molecular viscosity [$kg{\cdot}m^{-1}{\cdot}s^{-1}$]
ρ	density [kg m^{-3}]
τ	viscous stress tensor
$\vec{g}$	gravitational acceleration [$m{\cdot}s^{-2}$]
φ	phase potentials [V]

Acronyms

Ah	ampere - hour
BTMS	battery thermal management systems
CFD	computational fluid dynamics
DoD	depth of discharge
MSMD	multi-scale multi-dimensional
NTGK	Newman, Tiedemann, Gu, and Kim
SOC	state of charge
LIBs	lithium-ion batteries
WP	wetted perimeter

1P4S 1 parallel 4 series battery arrangement
C-rate the charge or discharge current with respect to the nominal capacity of a battery cell

2. Methodology

2.1. Battery modeling

For an accurate thermal analysis of a battery system, a three-dimensional model of the cell chemistry and associated physics is required to capture the internal heat flow paths and thermal resistance. At the battery cell's scale, the governing equation for the electric current flux is expressed as:

$$-\nabla \bullet (\sigma_+ \nabla \varphi_+) = \nabla \bullet (\sigma_- \nabla \varphi_-) = j \tag{1}$$

where σ_+ and σ_- are the effective electric conductivities for the positive and negative electrodes; φ_+ and φ_- are the phase potentials $[V]$ for the positive and negative electrodes; $j$is the volumetric current transfer rate in $[A \cdot m^{-3}]$ which is calculated in the electrochemical sub-model. In this study, the NTGK submodel was used due to its easy parameterization and effectiveness in modeling lithium-ion batteries. In the NTGK sub-model formulation, the volumetric current transfer rate j is related to the phase potentials using the following algebraic equation:

$$j = \frac{Q_{nom}}{Q_{ref} \bullet Vol} \cdot Y \cdot [U - (\varphi_+ - \varphi_-)\ ] \tag{2}$$

where Q_{nom} [Ah] is the battery's total capacity, Q_{ref} $[Ah]$ is the capacity of the battery used during the discharge experiment, Vol denotes the volume $[m^3]$ of the battery's active zone i.e. anode, cathode, and separator; Y $[\Omega^{-1}]$ and U $[V]$ are the model parameters which are obtained by curve fitting the voltage-current response curve obtained from experiments, Q_{ref} $[Ah]$ is the capacity of the battery used during the voltage-current response experiment. Y and U are functions of the battery depth of discharge (DoD):

$$DoD = \frac{Vol}{3600 Q_{nom}} \left(\int_0^t j dt \right) \tag{3}$$

$$Y = \left\{ \sum_{n=0}^{5} (DoD)^n \right\} exp\left\{ -C_1 \left(\frac{1}{T} - \frac{1}{T_{ref}} \right) \right\} \tag{4}$$

$$U = \left\{ \sum_{n=0}^{3} b_n (DoD)^n \right\} - C_2 (T - T_{ref}) \tag{5}$$

where Vol denotes the battery's active zone volume $[m^3]$, $Q_{nom}[AH]$ is the battery total electric capacity, T $[K]$ is the battery temperature, T_{ref} $[K]$ is the reference temperature, C_1 and C_2 are the battery specific NGTK constant, a_n is the coefficient of the Y polynomial, b_n is the coefficient of the U polynomial. In this study, the model parameters were obtained by fitting Eqs. (4) and (5) to experimental data of the LG CHM E66A cell discharged at 0.1C and 1C, as obtained from reference [30]. The specific fitting formulas can be expressed as:

$$\begin{aligned} U =& 4.179 - 1.694(DoD) + 4.135(DoD)^2 - 13.0925(DoD)^3 \\ &+ 19.7986(DoD)^4 - 10.449(DoD)^5 \end{aligned} \tag{6}$$

$$\begin{aligned} Y =& 1722.0 - 11736.7(DoD) + 47331.91(DoD)^2 - 79772.7(DoD)^3 \\ &+ 61703.45(DoD)^4 - 17204.9(DoD)^5 \end{aligned} \tag{7}$$

shows the predicted curves for the four discharge rates: 0.1C, 1C, 3C, and 5C compared with the experimental data [30]. The prediction shows a good agreement with the experimental data up to 3C; at 5C a slight deviation was observed at high SOC. Nonetheless, the NTGK model predicts the voltage response well and can provide the electrochemical

Table 1
Cell characteristics and geometry.

Cell format	Pouch
Dimension	354 mm × 101 mm × 11.7 mm
Weight	897.0 g
Capacity	65.0 Ah nominal, c/10 63.5 Ah
Current	Continuous 121A, peak 297A
Energy	c/10232.2 Wh
Power	Continuous 0.41KW, peak 1.04KW
Voltage range	2.5 V - 4.2 V

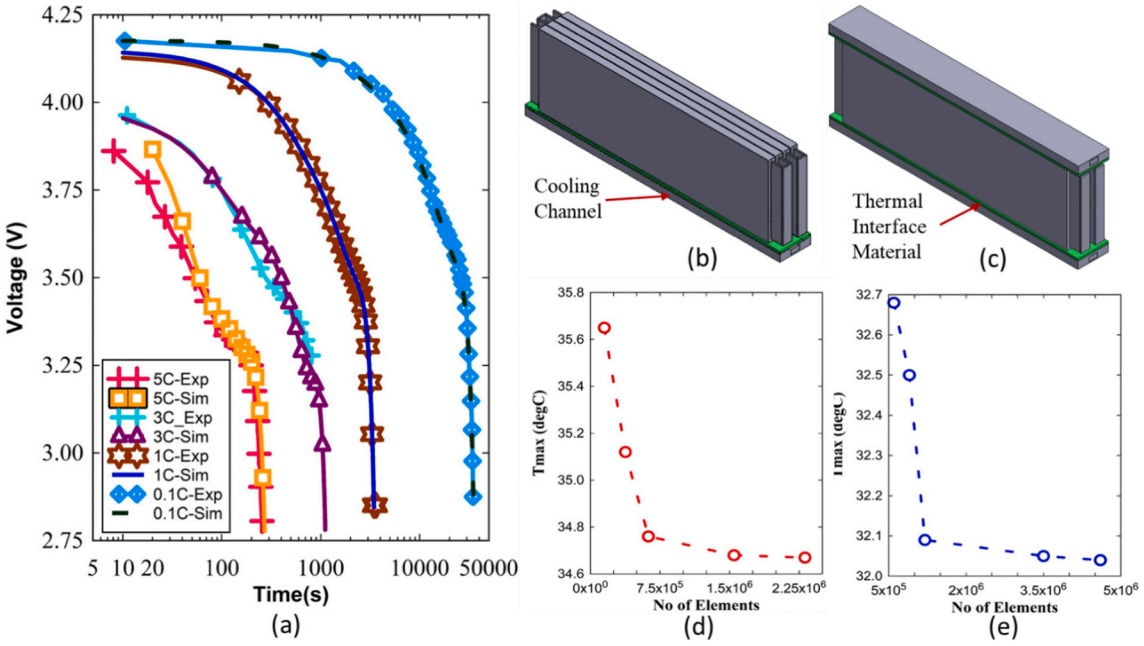

Fig. 1. (a) NGTK model voltage prediction vs experimental data during discharge with different battery discharge rates, (b) 1P4S module with a bottom cooling channel, (c) 1P4S module with top and bottom cooling channels, (d) Mesh independence study for 1P4S module with a bottom cooling channel, and (e) Mesh independence study for 1P4S module with top and bottom cooling channels.

Table 2
Thermal properties of the battery cell and silica gel pad.

Properties	Specific Heat Capacity, C_p [J·kg^{-1}·K^{-1}]	Thermal Conductivity, K [W·m^{-1}·K^{-1}]	Density, ρ [kg·m^{-3}]
Cell	954	Normal: 1.394 Plane: 28.706	2630.7
Silica gel pad	0.832	3.000	1071.1
Aluminum	871	202.4	2719
Copper	381	387.6	8978

characteristics for the battery model under study. The electrochemical volumetric heat generation, $\dot{Q}_{ECh}$ [W·m^{-3}] by the battery during cell discharge can then be expressed as:

$$\dot{Q}_{ECh} = j\left[U - (\varphi_+ - \varphi_-) - T\frac{dU}{dT}\right] \tag{8}$$

where $j[U - (\varphi_+ - \varphi_-)]$ is the irreversible over-potential heat generated in [W·m^{-3}] and $-jT\frac{dU}{dT}$ [W·m^{-3}] is the reversible entropic heating due to exothermic and endothermic reactions within the cell during charge/discharge. The total heat generated $\dot{Q}_{total}[W]$ is then given by:

$$\dot{Q}_{total} = \dot{Q}_{ECh} + \frac{\dot{Q}_{ohm}}{Vol} \tag{9}$$

Ohmic heat, $\dot{Q}_{ohm}$[W], generated is defined as:

$$\dot{Q}_{ohm} = \sigma_+|\nabla\varphi_+|^2 + \sigma_-|\nabla\varphi_-|^2 \tag{10}$$

To determine the battery's temperature distribution (T), the energy equation is solved with the source term:

Table 3
1P4S module super charging profile.

	C-Rate	Current (A)	Charging time (s)	Charging capacity (Ah)
1	1.98	128.7	1330	47.54
2	1.89	122.85	1440	49.14
3	1.75	113.75	1620	51.18
5	1.48	96.2	2060	55.04
6	1.30	84.5	2440	57.27

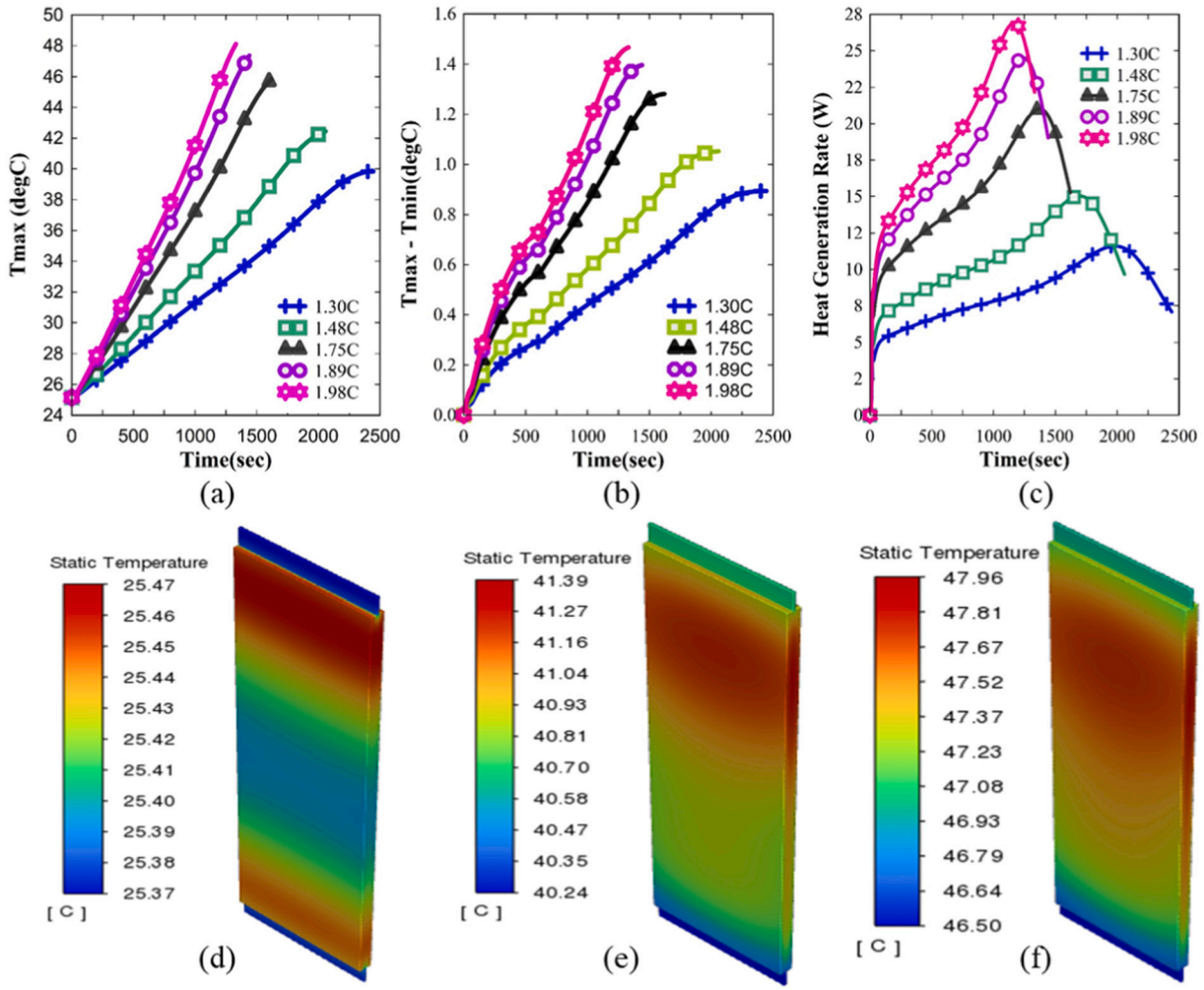

Fig. 2. Constant current charging of a single cell showing (a) maximum temperature, (b) temperature difference, and (c) heat generation rate. The temperature distribution during 1.98C charging of a single cell is shown at timesteps: (d) the 50s (e) 1000s (f) 1330s.

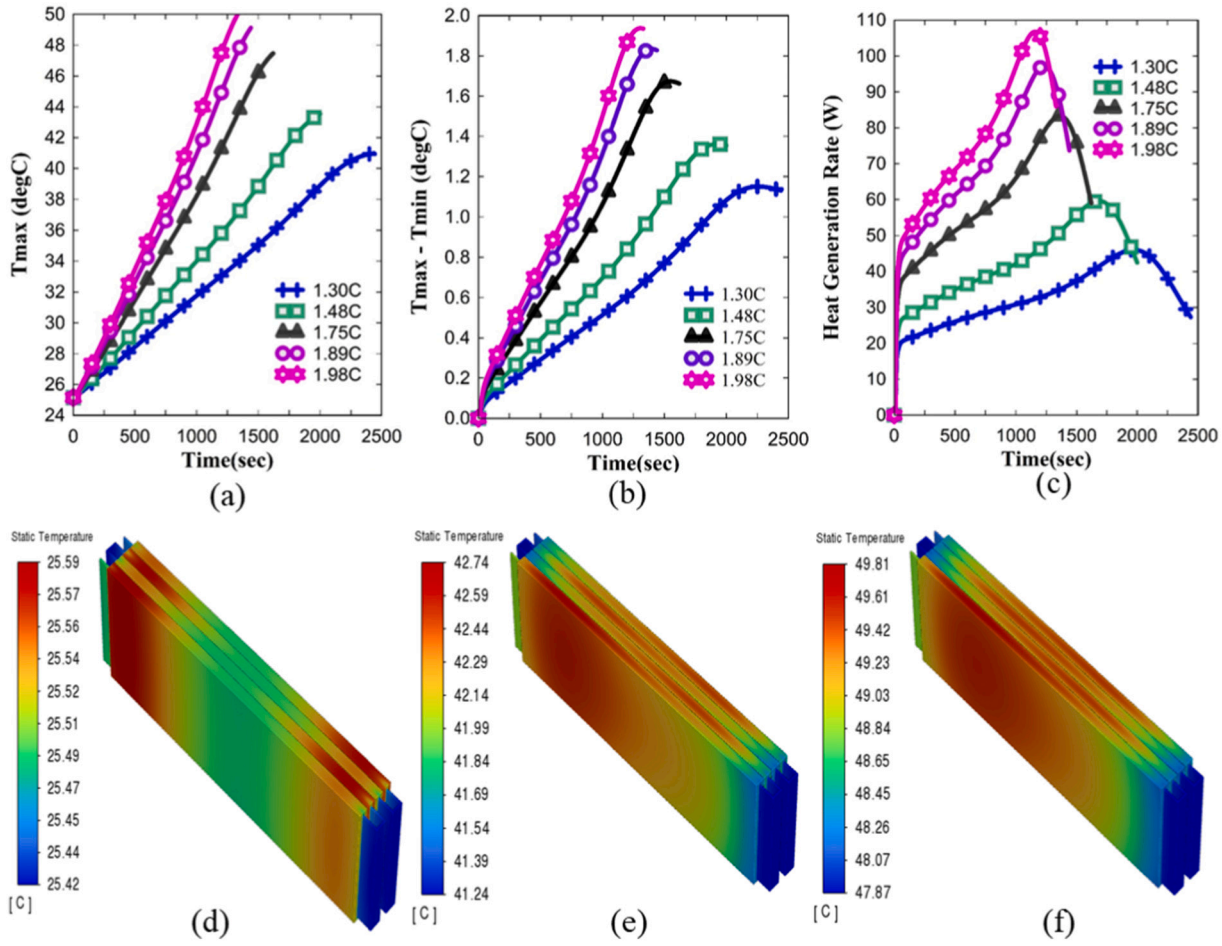

Fig. 3. Comparison of 1P4S (a) Maximum temperature, (b) Temperature difference, and (c) Heat generation rate at different C-rates during ambient cooling. Temperature distribution of 1P4S during 1.98C charging with ambient cooling at (a) 50s (b) 1000s (c) 1330s.

Table 4
1P4S cooling channel properties.

Top plate thickness	3 mm
Coolant channel	351 mm × 40 mm × 6 mm
Bottom plate thickness	1.5 mm
Material	Aluminum
Inlet temperature	25 °C
Coolant	Water

$$\frac{\partial \rho C_p T}{\partial t} - \nabla \bullet (k \nabla T) = \dot{Q}_{total} \tag{11}$$

where ρ, C_p, k are the density [kg·m^{-3}], specific heat capacity [J·Kg^{-1}·K^{-1}], and the thermal conductivity [W·m^{-1}·K^{-1}] of the battery, respectively. These parameters are calculated using a weighted average of the values for each element making up the active material i.e. positive current collector, positive electrode, separator, negative electrode, and negative current collector, such that:

$$\rho = \frac{\sum_{i=1}^{n} \rho_i \delta_i}{\delta_c} \tag{12}$$

$$C_p = \frac{\sum_{i=1}^{n} C_{p_i} \rho_i \delta_i}{\rho \delta_c} \tag{13}$$

$$k = \frac{\sum_{i=1}^{n} k_i \delta_i}{\delta_c} \tag{14}$$

where n is the number of elements, and δ_c is the thickness of the cell in meter*(m)*. For model simplification, the following assumptions were made:

1. Only conduction and convective heat transfer are considered, as radiation is insignificant due to the battery cell being an opaque system.
2. Coolant is assumed to be incompressible.
3. Thermophysical properties of the battery: specific heat capacity, thermal conductivity, and density, were assumed to be independent of time.
4. Friction losses in the cooling channel are ignored.
5. Coolant flow is assumed to be laminar and fully developed.
6. Contact resistance between cells and cooling plate(s) is ignored.

2.2. Conjugate heat transfer

For cooling the battery with fluid, a conjugate heat transfer problem is formulated. Firstly, it must be determined if the coolant flow is laminar or turbulent. Reynold's number for the coolant is calculated using:

$$Re = \frac{\rho_C V D_h}{\mu} \tag{15}$$

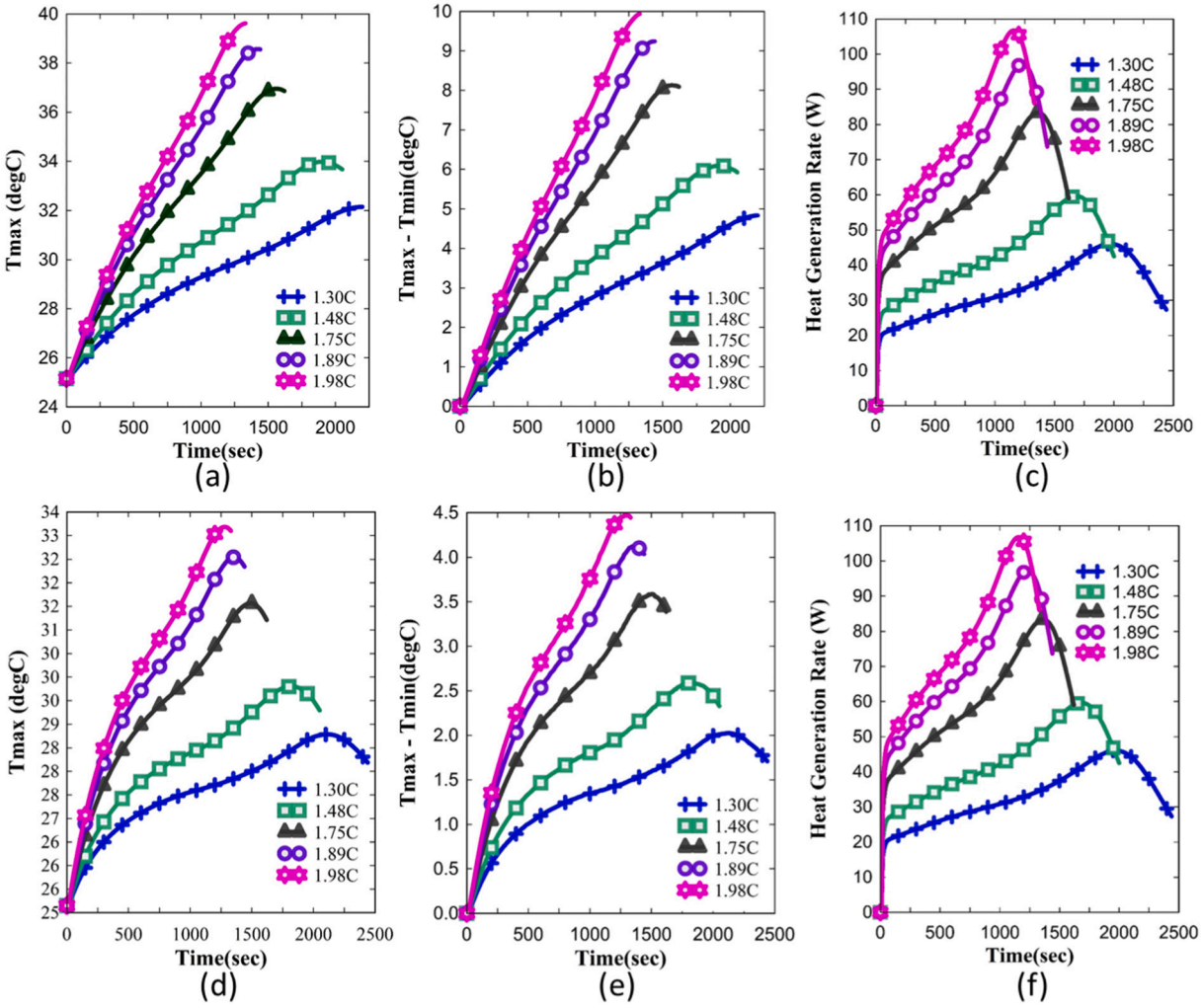

Fig. 4. Bottom cooling of 1P4S module showing: (a) maximum temperature, (b) temperature difference, and (c) heat generation rate for different C-rates. Top and bottom cooling of 1P4S module showing: (d) maximum temperature, (e) temperature difference, and (f) heat generated for different C-rates.

where ρ_C is the coolant density in V is the fluid's inlet velocity [m·s^{-1}], μ is the fluid's dynamic viscosity [kg·m^{-1}·s^{-1}] and D_h is the hydraulic diameter [m] calculated using the:

$$D_h = \frac{4A_c}{WP} \tag{16}$$

where A_c is the cross-sectional area [m^2] of the cooling channel and WP [m] is the wetted perimeter. In this work, a laminar flow is assumed and the following governing equations are solved numerically using ANSYS Fluent software:

$$\text{Continuity Equation}: \frac{\partial \rho_C}{\partial t} + \nabla \bullet \left(\rho_C \vec{V}\right) = 0 \tag{17}$$

$$\text{Momentum Equation}: \frac{\partial \left(\rho_C \vec{V}\right)}{\partial t} + \nabla \bullet \left(\rho_C \vec{V}\vec{V}\right) = -\nabla p + \nabla(\tau) + \rho_C \vec{g} \tag{18}$$

where t is time, $\vec{V}$ is the velocity vector of coolant [m·s^{-1}], ρ_C is the density of coolant [Kg·m^{-3}], p is the pressure [Pa], $\vec{g}$ is the gravitational acceleration [m·s^{-2}], and τ is the viscous stress tensor [Pa]. The continuity equation is solved to give the velocity of the fluid while the momentum equation gives the pressure.

2.3. Computation scheme

The cooling plate and battery cells were discretized using ANSYS Fluent Meshing R21.2 with the unstructured meshing of the polyhedral type. The mass flow inlet boundary condition was employed at the inlet and a gage pressure of 0 kPa was set for the outlet boundary condition. The exposed boundaries of the battery and cold plate were set as convective boundary conditions with a constant heat transfer coefficient of 5 W·m^{-2}·K^{-1}. No slip boundary condition was also specified at the fluid-wall interface. To model the heat conduction at the interfaces, a coupled wall was used. Thermal resistance at the interfaces was ignored; also, radiation heat losses were not considered.

2.4. Mesh independence study

To have confidence in the results of the analysis, a mesh independence study was carried out. The goal of the mesh study was to verify that the mesh number (or discretization) chosen does not affect the simulation results. For this, different mesh numbers were used for a condition where the inlet temperature was 30 °C, the ambient temperature was 40 °C and the battery's initial temperature was 35 °C. The results of the mesh study are shown in Fig. 1(d) and Fig. 1(e) for both bottom-only cooling assembly and bottom and top cooling assembly, respectively. The maximum temperature was at 1.4 × 10^6 number of elements for the bottom cooled assembly and 3.5 × 10^6 number of

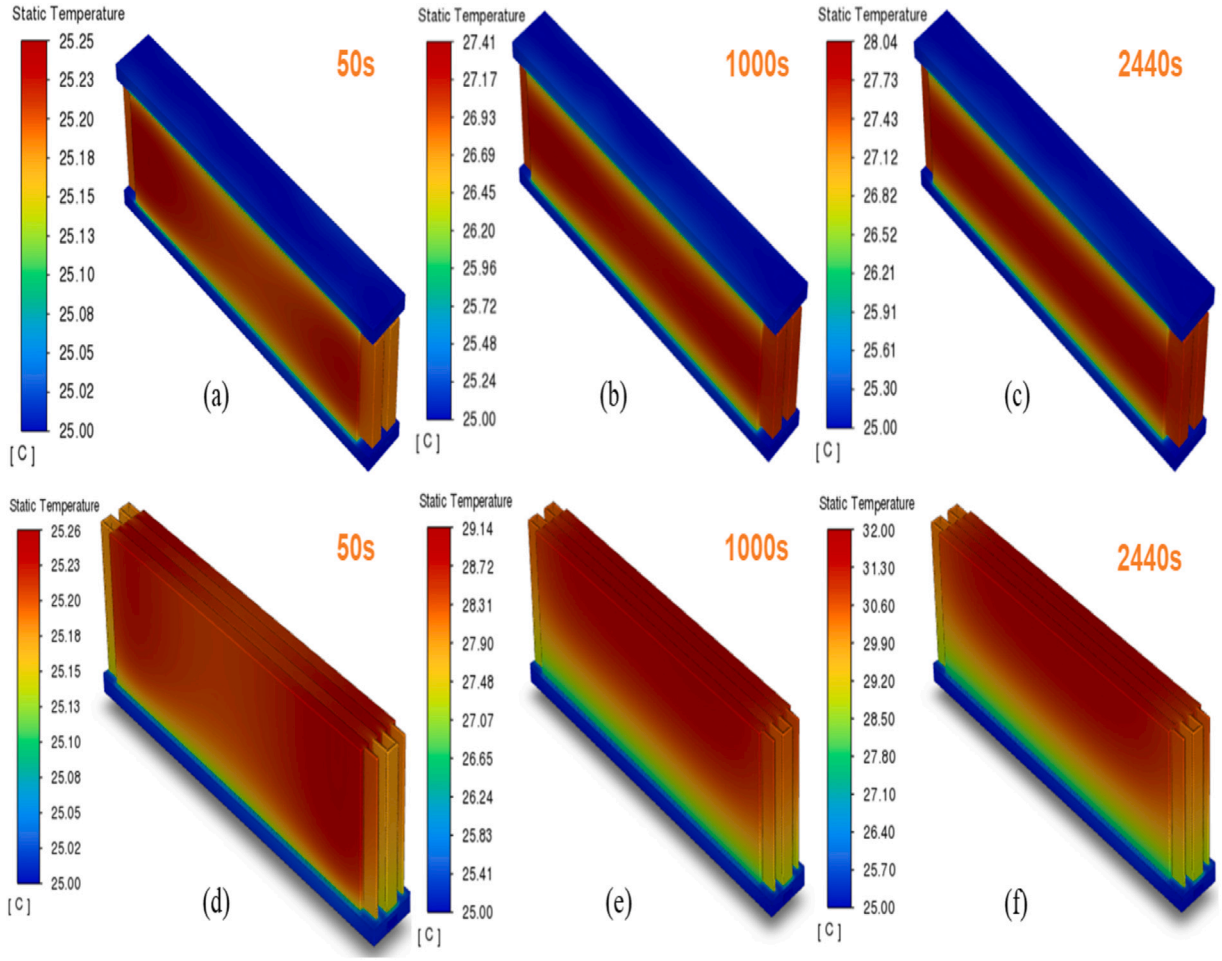

Fig. 5. Temperature distribution of 1P4S during 1.30C charging at (a) 50 s, (b) 1000 s (c) 2440 s with top and bottom side cooling channels. Temperature distribution of 1P4S during 1.30C charging at (d) 50 s (e) 1000 s and (f) 2440 s with only bottom side cooling.

elements for the bottom and top cooled assembly; thus, these settings were used for the different simulations that follow. The model validation was carried out by comparing the experiment results by the manufacturer to the simulation setup. The symbols listed in Fig. 1(a) show the experimental data and generated lines generated by our simulations.

2.5. Battery specification

The battery cell used in this study is a commercially available LG CHEM E66A with specifications given in Table 1.

[30].

For the single-cell study, the cell was modeled in Solidworks with three distinct regions: an active region (cell) and two passive regions (positive tab and negative tab). The module is made by combining four cells with bus bars in series to create the 1P4S pack configuration as shown in Fig. 1(b). The cooling system is a single-pass, rectangular-duct channel comprised of a single inlet and outlet as shown in Fig. 1(b). To enhance heat transfer between the battery cells and the cooling channel, a silica gel pad is used as a thermal interface material [31] between the cooling channel and the 1P4S module as shown in Fig. 1(c). The thermal properties of the cell and the silica gel pad are given in Table 2.

3. Results and discussion

3.1. Single-cell charging with ambient convective cooling

The thermal characteristic of a single cell under different charging conditions is considered first. Thermal properties listed in.

are used for the active part of the cell while the positive and negative tabs are made from aluminum and copper, respectively. Using a natural convection heat transfer coefficient of 5 $W{\cdot}m^{-2}{\cdot}K^{-1}$ and convective boundary condition on the battery surface only, the model was simulated with polyhedral mesh and 128,909 mesh elements and results are shown in Fig. 2. As shown in Fig. 2(a–c), charging at 1.98C gave the highest cell temperature of 49 °C, highest heat generation rate of around 27 W, and with a temperature difference of <2 °C. As the C-rates drop to 1.30C, the maximum temperature, temperature difference, and heat generated reduce almost linearly. Since both maximum temperature and temperature difference have a significant effect on the battery performance and degradation, a cooling system is needed to keep them within an optimum range of <5 °C for temperature difference and between 30 °C and 45 °C for maximum temperature, particularly during fast charging cycles. The temperature distribution during charging at 1.98C is shown in Fig. 2(d-f) at time intervals of the 50s, 1000s, and at end-of-charge. It shows that during single-cell charging, the hottest region starts close to the negative tab and grows into the center of the cell, eventually the side edges recorded the maximum cell temperature, similar to the results from references [7,32] for temperature distribution in a pouch cell with opposing tabs. The temperature evolution also showed that the region closest to the negative copper tabs had a higher temperature than the region near the positive aluminum tabs at the early stage of charging. This might be due to the negative tab material having a higher thermal conductivity than the positive tab material since a similar distribution was observed when the cell was discharged at the same rate.

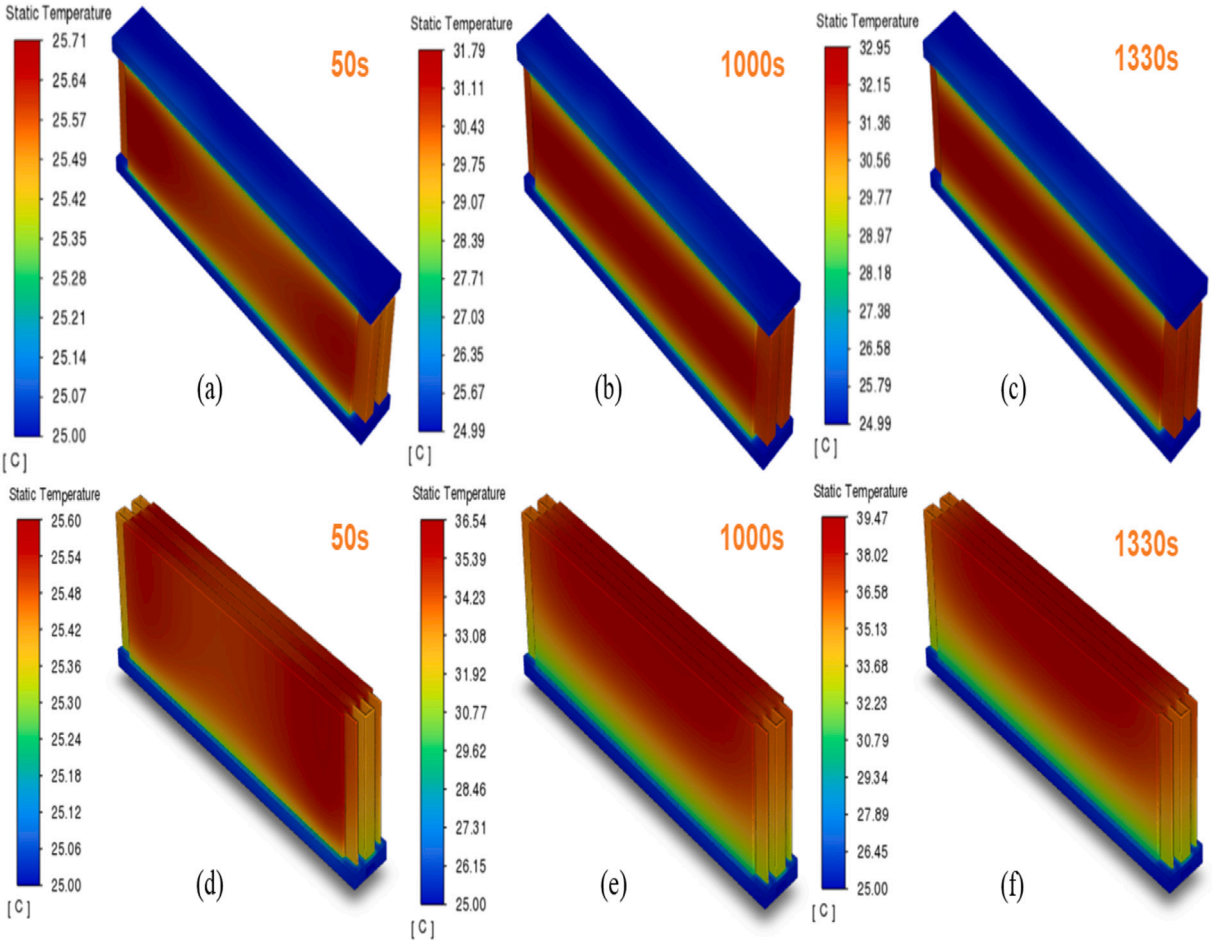

Fig. 6. Temperature distribution of 1P4S during 1.98C charging with coolant cooling at (a) 50 s, (b) 1000 s, and (c) 1330 s with top and bottom cooling channels. Temperature distribution of 1P4S during 1.30C charging at (d) 50 s, (e) 1000 s, and (f) 1330 s with the only bottom cooling channel.

For the single cell considered here, the maximum temperature increased as the charging rate increases, this is a significant limitation for fast charging applications.

3.2. 1P4S fast charging study

For the fast charging study, a module made up of four cells as shown in Fig. 1(b) is utilized. The resulting module possesses a combined voltage of 16.8 V and a total battery capacity of 260 Ah. During fast charging, a high current or voltage is impacted the battery within a short timeframe. In this study, constant current charging is used. Doing this drives up the temperature of the battery module; as the charging process progresses, the higher temperature experienced leads to faster electrochemical reactions which in turn generate more heat and lead to a still higher temperature. The goal of this study is to explore the battery thermal characteristics during both natural convection ambient cooling and forced convection liquid cooling conditions. Here, the thermal system would need to satisfy the following constraints:

1. $T_{max} \leq 45\ ^{\circ}C$.
2. $T_{max} - T_{min} \leq 5\ ^{\circ}C$.

First, the ambient cooling (natural convection) condition is explored, followed by forced convection cooling on one side of the module, then forced convection cooling on both sides of the module. All studies use the charging profiles listed in Table 3.

3.2.1. 1P4S fast charging study with ambient convective cooling

The study of the thermal behavior of the battery module under a natural convective heat transfer coefficient of 5 $W{\cdot}m^{-2}{\cdot}K^{-1}$ and an ambient temperature of 25 °C was carried out. The battery was assumed to be at thermal equilibrium at the beginning of the experiment, thus the initial battery temperature was 25 °C; the simulation stops once the maximum cut-off voltage of 4.2 V is reached. The model domain was discretized into 600,000 mesh elements at which point the solution showed a negligible difference in average temperature. Thermal analysis results under ambient cooling conditions are shown in Fig. 3.

As shown in Fig. 3(a-c), the maximum temperature and heat generation rate increases with increasing C-rate, with a peak temperature of 50 °C and heat generation rate of 108 W registered during 1.98C charging. Despite the high calculated peak temperatures, the temperature differences were all found to be below 2 °C. This temperature uniformity is attributed to the fact that the walls of the battery experience the same convective cooling as defined by the boundary wall condition used in the model, i.e. the heat loss from the battery is uniform across all the cells, therefore the thermal gradient is caused mainly by the ohmic heat due to flow of current in the cells, tabs, and busbars. The rapid heat generation rate coupled with the low convective heat removal in ambient cooling conditions can enhance uniform temperature distribution but results in a large cell temperature increase which can trigger thermal runaway and enhanced cell degradation. The temperature distribution at the 50s, 1000s, and end-of-charge (EOC) points for 1.98C only are shown in Fig. 3(d-f). The results show that the maximum temperature occurs along the edges of the cell close to the negative tab; this may be due to the orthotropic thermal conductivity defined for the active cell while the lowest temperature regions are at the tabs and connectors. The result from this study serves as a reference point for which the proposed forced convection cooling system can be compared.

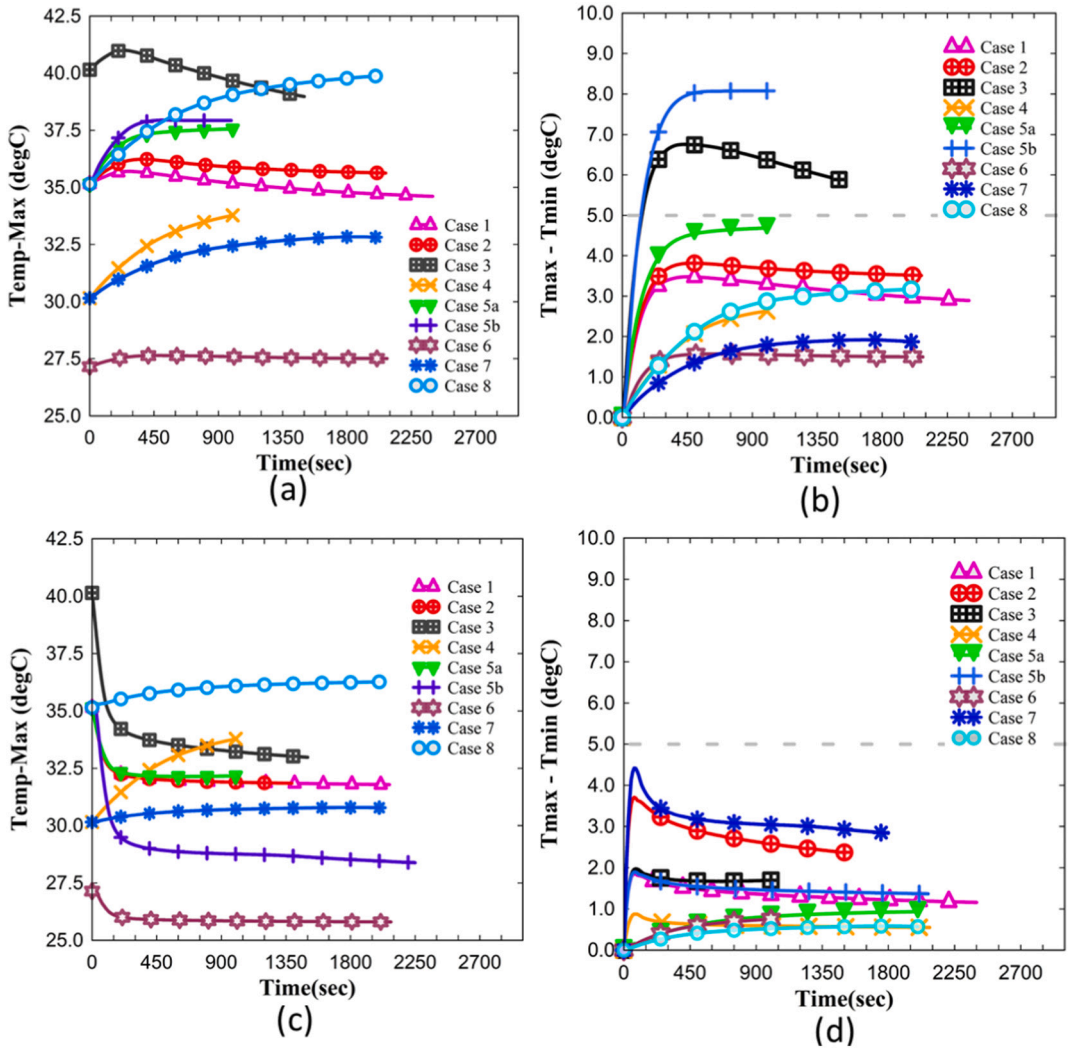

Fig. 7. Bottom-cooled assembly showing: (a) maximum temperature in the module, (b) temperature difference in the module, (c) maximum temperature on the surface of the cooling plate, and (d) temperature difference on the surface of the cooling plate.

3.2.2. 1P4S fast charging with liquid cooling on one side

A cold plate of height 10.5 mm was placed at the bottom of the battery module as shown in Fig. 1(b) and the inlet mass flow rate was set at 0.33 kg/s. For this study, only one inlet temperature of 25 °C was considered and the flow was assumed to be laminar. The properties of the cooling system are given in Table 4. The maximum element size used for the polyhedral unstructured meshes is 0.5 mm for the 3 mm thick silica gel pad and the other components were constrained to a maximum element size of 2.5 mm which gave a total of 1,471,058 elements used for this simulation.

The temperature distribution of the 1P4S module with bottom cooling channel at different times during 1.30C and 1.98C is shown in Fig. 5(b-d) and Fig. 6(b-d), respectively. The simulation results showed that the maximum temperature was reduced significantly by up to 10 °C, compared to ambient cooling, for all cases considered by cooling from the side edges of the battery as shown in Fig. 4(a). However, the temperature difference has increased substantially with a difference of up to 10 °C during 1.98C and 5 °C during 1.30C in the module as shown in Fig. 4(b). This thermal non-uniformity is a catalyst for inhomogeneous lithium plating in the LIB cells [33]. This is expected as the flowing water at the bottom was able to cool up the part of the battery next to the cooling channel while the other end of the cell is still under ambient cooling. Thus, such one-sided cooling set up a significant thermal gradient in the battery with the consequence that the temperature difference has gone up compared to ambient cooling. The implication of this for the EV industry seeking to achieve faster charging rate in the >2C regime is that such one-sided cooling will not guarantee a safer and longer lasting battery module. To achieve thermal balance, at least two opposed cooling channels or plates should be used. In the next section, this approach is studied.

3.2.3. 1P4S fast charging with liquid cooling on both sides

The model used for this study is shown in Fig. 1(c). The cooling channel is placed on the top and bottom of the 1P4S module with the silica gel pad at the interface between the battery and the cooling channel. To guarantee thermal balance an opposing flow arrangement is used where the inlet of the lower cooling channel lies on the same side as the outlet of the upper cooling channel. The result shown in Fig. 4 gives the comparison of the thermal behavior of cooling one side of the battery versus cooling both sides of the battery. By cooling both sides of the 1P4S module, the maximum temperature difference reached was 4.5 °C at 1.98C as shown in Fig. 4(e). In contrast, a temperature difference of 10 °C was recorded when only the bottom side was cooled at a charging rate of 1.98C as shown in Fig. 4(b). Also, the maximum temperature has reduced from about 40 °C to 33 °C for 1.98C; however, as the C-rates decrease the savings were not very noticeable with charging at 1.30C only seeing a reduction of 4 °C in maximum temperature. As shown in Fig. 5(a) and Fig. 5(c), the hot spot during two-sided cooling occurs at

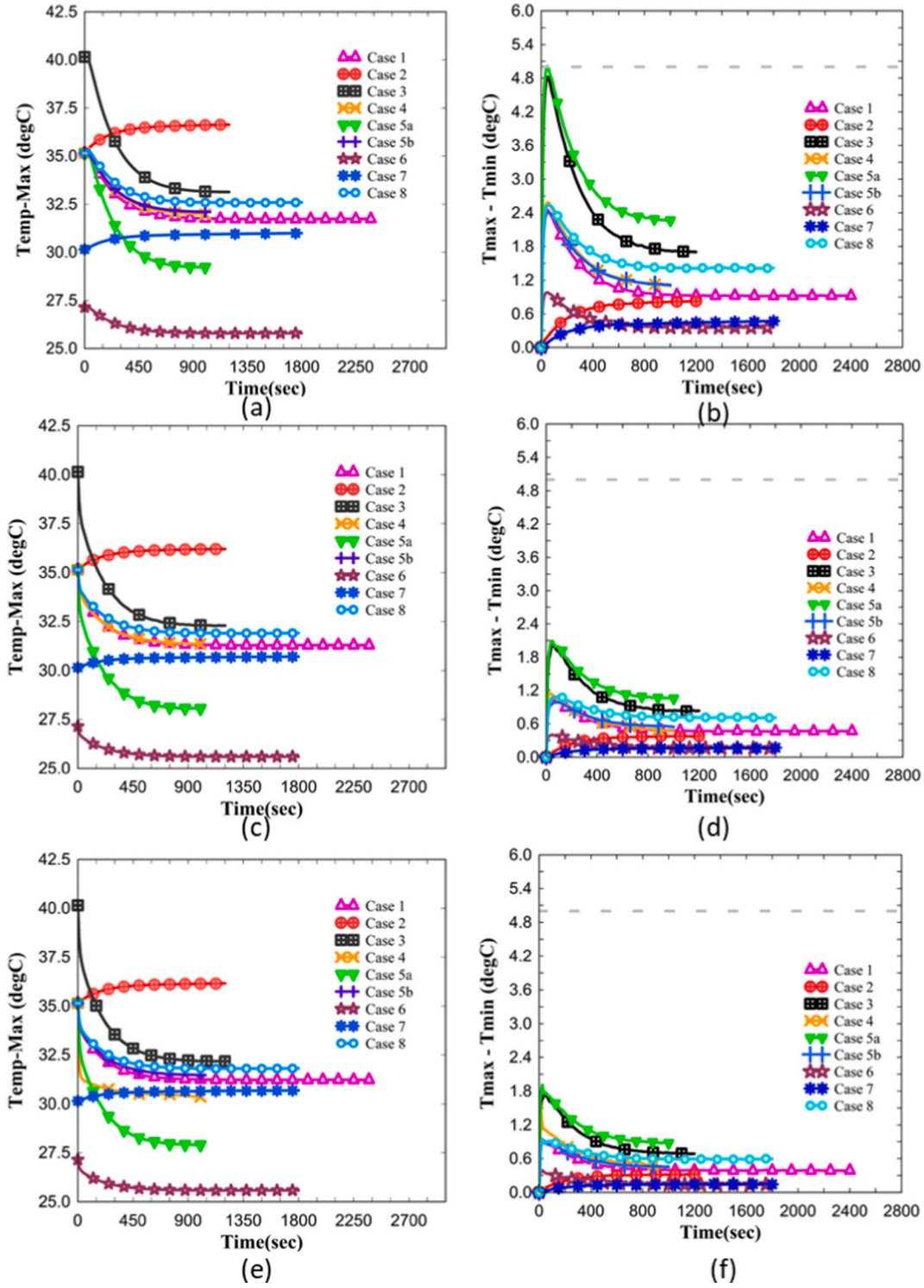

Fig. 8. Bottom and top cooled assembly showing: (a) module maximum temperature, (b) module temperature difference, (c) top plate maximum temperature, (d) top plate temperature difference, (e) bottom plate maximum temperature, and (f) bottom plate temperature difference.

the center of the cell along the coolant flow direction. Compared to one-side cooling the maximum temperature difference reduced significantly from about 10 °C during 1.98C with one-side cooling to 4.5 °C during 1.98C with two-side cooling. This shows the benefit of cooling both edges of the battery module compared to just one edge.

3.3. Multiple driving cases

To assess the thermal performance of the two cooling plate designs under varied charging and environmental conditions, multiple case profiles as shown in Table 5 were used. In cases 1–4, the coolant's inlet temperature was fixed at 30 °C while the battery was charged by an external charger for different periods. In case 5, two different coolant temperatures were evaluated at the same battery and ambient

Table 5
Profiles of multiple driving conditions used to evaluate the thermal performance of single-channel and double-channel designs for 1P4S cooling.

Vehicle charging conditions	Ambient temp (°C)	Time (sec)	Battery initial temp (°C)	Coolant mass flow rate (kg/ s)	Coolant temp. (°C)	Battery power (kW)
Case 1	40	2400	35	0.33	30	1.37
Case 2	40	1200	35		30	2.31
Case 3	45	1200	40		30	2.50
Case 4	40	1000	35		30	1.98
Case 5	40	1000	35		(a) 25 (b) 30	3.59
Case 6	27	1800	27		25	1.53
Case 7	30	1800	30		30	2.22
Case 8	45	1800	35		35	1.78

conditions. Cases 6–8 have different coolant temp and ambient temperatures, but the battery was charged for the same period. The evaluation conditions limit the maximum temperature to only 45 °C and the temperature difference should be <5 °C.

As shown in Fig. 7(a), when a single channel cooling was used, the maximum temperatures attained for all the cases were below the design maximum of 45 °C. Also, for cases 5a and 5b, where the coolant temperature was 25 °C and 30 °C, the maximum temperature increased accordingly with Case 5a reaching a maximum of 37.5 °C, while Case 5b reached a maximum of 37.9 °C. This is expected since the higher coolant temperature means Case 5b could not remove as much heat as Case 5a from the battery cells. However, for the temperature difference as shown in Fig. 7(b), Case 5b and Case 3 were above the 5 °C limit set for the maximum temperature difference. For these two cases, the higher initial battery temperature and coolant temperature implied that for the current design a single channel could not remove the heat fast enough to achieve a more uniform thermal distribution in the battery cells. However, when two channels were used, as shown in Fig. 8(a), the maximum temperature reduced at a faster rate compared to Fig. 7(a) as the rate of heat removal from the module was higher. Also, the temperature difference target of <5 °C was achieved for all the cases considered as shown in Fig. 8(b). For most of the cases, the temperature difference was below 3 °C, except for the extreme cases – Case 5a and Case 3 which were close to the design target of 5 °C. The maximum temperature observed in the top and bottom cooling planes were identical as shown in Fig. 8(c) and Fig. 8(e), this is because the heat generation in the battery cell and heat removal from the top and bottom are similar across the module. A similar observation was noted for the temperature difference as shown in Fig. 8(d) and Fig. 8(f), where the maximum temperature difference in the top and bottom planes for all the cases showed similar evolution over the simulation duration. These results showed that the top and bottom plates can keep the battery modules within the design's maximum temperature and temperature difference. This is an interesting result as one of the greatest constraints to achieving faster charging rate is maintaining thermal uniformity and reducing thermal hotspot. Our result showed by using two opposing plates the thermal gradients can be significantly reduced.

The simulation results can provide insight into the design of the battery pack. The results can be used to optimize the design of the battery pack, taking into consideration the heat generation, heat transfer, and cooling requirements. This can result in better battery performance, longer battery life, and improved safety. The simulation results can be used to optimize the thermal management system for the battery pack. This can help to ensure that the battery is kept within its safe operating temperature range and prevent thermal runaway. Effective thermal management can also reduce charging time and improve the overall performance of the battery. The simulation results can help to optimize the manufacturing process for the battery pack. The results can be used to identify the optimal placement of the battery cells and cooling channels, which can improve the efficiency of the manufacturing process and reduce costs. The simulation results can be used to develop test protocols for the battery pack. By simulating the battery under various conditions, engineers can develop test procedures that more accurately reflect the real-world performance of the battery. In conclusion, the thermal simulation results for an electric vehicle battery can have significant implications for the industry. By providing insights into battery design, thermal management, manufacturing, and testing, these results can help to improve the performance, reliability, and safety of electric vehicles, which is crucial for the wider adoption of electric vehicles in the future.

4. Conclusion

The study developed a battery thermal model for electric vehicle fast charging cycles using the NGTK model in ANSYS Fluent, and the simulated model was compared with experimental data to validate the accuracy of the model. The study focused on the cooling performances of different cooling configurations, including single cell with ambient cooling, 1P4S module with a one-side liquid cooling system, and 1P4S module with a two-sided liquid cooling system, using an electrochemical-thermal simulation approach. The study found that ambient convective cooling produced a high maximum temperature in the cells, but with a more uniform temperature distribution compared to forced convection cooling cases. The study recommended that EV companies consider the double-sided cooling approach, especially when designing fast-charging batteries that have high potentials for generating significant local thermal hotspot and thermal gradient. The simulation confirmed that the use of a one-sided cooling system with water as the coolant significantly reduced the battery temperature, but also caused a significant thermal gradient, which could lead to battery degradation and accelerated aging. By cooling the module on both sides, the temperature difference and maximum temperature were kept within the design operating range. The study confirmed this by performing a case study on the battery with different environmental and operating conditions subjected to multiple charging rates. The multi-case study confirmed that the top and bottom plate cooling configuration can keep the battery modules within the allowable maximum temperature and temperature difference design constraints. The implication of this study for the industry is significant, as it highlights the importance of effective thermal management in the design of electric vehicle batteries, particularly for fast-charging batteries. The use of multidomain modeling and simulation approaches can help battery manufacturers optimize the design of their battery packs to improve thermal management, reduce the risk of thermal runaway, and improve battery performance and longevity. By adopting double-sided cooling approach, EV companies can design more reliable and efficient batteries, which can help to accelerate the adoption of electric vehicles worldwide.

CRediT authorship contribution statement

Ayodeji Adeniran: Conceptualization, Methodology, Writing – original draft. **Sam Park:** Supervision, Writing – original draft, Writing – review & editing.

Declaration of competing interest

The authors declare that they have no known competing financial interests or personal relationships that could have appeared to influence the work reported in this paper.

Data availability

Data will be made available on request.

Acknowledgement

This work was supported by the NSF: IUCRC (EVSTS: # 2147117) and Brain Pool Program through the Korean Federation of Science and Technology Societies (KOFST) funded by the Ministry of Science and ICT, Korea (2022H1D3A2A0105549111).

References

[1] M. Farag, H. Sweity, M. Fleckenstein, S. Habibi, Combined electrochemical, heat generation, and thermal model for large prismatic lithium-ion batteries in real-time applications, J. Power Sources 360 (2017) 618–633, https://doi.org/10.1016/j.jpowsour.2017.06.031.

[2] J. Zhao, Z. Rao, Y. Huo, X. Liu, Y. Li, Thermal management of cylindrical power battery module for extending the life of new energy electric vehicles, Appl. Therm. Eng. 85 (2015) 33–43, https://doi.org/10.1016/j.applthermaleng.2015.04.012.

[3] A. S. S. Pesaran G. H. Kim , "Addressing the impact of temperature extremes on large format Li-ion batteries for vehicle applications," Presented at the 30th International Battery Seminar Ft. Lauderdale, Florida, 2013, Ft. Lauderdale, Florida.

[4] X. Tan, P. Lyu, Y. Fan, J. Rao, K. Ouyang, Numerical investigation of the direct liquid cooling of a fast-charging lithium-ion battery pack in hydrofluoroether, Appl. Therm. Eng. 196 (2021), https://doi.org/10.1016/j.applthermaleng.2021.117279.

[5] T. Deng, G. Zhang, Y. Ran, P. Liu, Thermal performance of lithium ion battery pack by using cold plate, Appl. Therm. Eng. 160 (2019), https://doi.org/10.1016/j.applthermaleng.2019.114088.

[6] T.M. Bandhauer, S. Garimella, T.F. Fuller, A critical review of thermal issues in lithium-ion batteries, J. Electrochem. Soc. 158 (3) (2011) pp, https://doi.org/10.1149/1.3515880.

[7] X. Zhang, X. Chang, Y. Shen, Y. Xiang, Electrochemical-electrical-thermal modeling of a pouch-type lithium ion battery: an application to optimize temperature distribution, J. Energy Storage 11 (2017) 249–257, https://doi.org/10.1016/j.est.2017.03.008.

[8] R. Mahamud, C. Park, Reciprocating air flow for Li-ion battery thermal management to improve temperature uniformity, J. Power Sources 196 (13) (2011) 5685–5696, https://doi.org/10.1016/j.jpowsour.2011.02.076.

[9] T. Wang, K.J. Tseng, J. Zhao, Z. Wei, Thermal investigation of lithium-ion battery module with different cell arrangement structures and forced air-cooling strategies, Appl. Energy 134 (2014) 229–238, https://doi.org/10.1016/j.apenergy.2014.08.013.

[10] I.A. Hunt, Y. Zhao, Y. Patel, J. Offer, Surface cooling causes accelerated degradation compared to tab cooling for lithium-ion pouch cells, J. Electrochem. Soc. 163 (9) (2016) A1846–A1852, https://doi.org/10.1149/2.0361609jes.

[11] A. Jarrett, I.Y. Kim, Design optimization of electric vehicle battery cooling plates for thermal performance, J. Power Sources 196 (23) (2011) 10359–10368, https://doi.org/10.1016/j.jpowsour.2011.06.090.

[12] A. Bhattacharjee, R.K. Mohanty, A. Ghosh, Design of an optimized thermal management system for Li-ion batteries under different discharging conditions, Energies 13 (21) (2020), https://doi.org/10.3390/en13215695.

[13] C. Lin, S. Xu, G. Chang, J. Liu, Experiment and simulation of a LiFePO4 battery pack with a passive thermal management system using composite phase change material and graphite sheets, J. Power Sources 275 (2015) 742–749, https://doi.org/10.1016/j.jpowsour.2014.11.068.

[14] F. Samimi, A. Babapoor, M. Azizi, G. Karimi, Thermal management analysis of a Li-ion battery cell using phase change material loaded with carbon fibers, Energy 96 (2016) 355–371, https://doi.org/10.1016/j.energy.2015.12.064.

[15] H. Behi, et al., Thermal management analysis using heat pipe in the high current discharging of lithium-ion battery in electric vehicles, J. Energy Storage 32 (2020), https://doi.org/10.1016/j.est.2020.101893.

[16] R.D. Jilte, R. Kumar, M.H. Ahmadi, L. Chen, Battery thermal management system employing phase change material with cell-to-cell air cooling, Appl. Therm. Eng. 161 (2019), https://doi.org/10.1016/j.applthermaleng.2019.114199.

[17] M.M.Kenneth J. Kelly, Matthew Zolot, Battery usage and thermal performance of the Toyota Prius and Honda insight for various chassis dynamometer testing, in: Presented at the Battery Conference on Applications & Advances Long Beach, California, 2002.

[18] M.S. Patil, J.H. Seo, S. Panchal, M.Y. Lee, Numerical study on sensitivity analysis of factors influencing liquid cooling with double cold-plate for lithium-ion pouch cell, Int. J. Energy Res. 45 (2) (2020) 2533–2559, https://doi.org/10.1002/er.5946.

[19] Y. Huo, Z. Rao, X. Liu, J. Zhao, Investigation of power battery thermal management by using mini-channel cold plate, Energy Convers. Manag. 89 (2015) 387–395, https://doi.org/10.1016/j.enconman.2014.10.015.

[20] K. Monika, C. Chakraborty, S. Roy, R. Sujith, S.P. Datta, A numerical analysis on multi-stage tesla valve based cold plate for cooling of pouch type Li-ion batteries, Int. J. Heat Mass Transf. 177 (2021), https://doi.org/10.1016/j.ijheatmasstransfer.2021.121560.

[21] L. Sheng, et al., Numerical investigation on a lithium ion battery thermal management utilizing a serpentine-channel liquid cooling plate exchanger, Int. J. Heat Mass Transf. 141 (2019) 658–668, https://doi.org/10.1016/j.ijheatmasstransfer.2019.07.033.

[22] W. Kong, K. Zhu, X. Lu, J. Jin, M. Ni, Enhancement of lithium-ion battery thermal management with the divergent-shaped channel cold plate, J. Energy Storage 42 (2021), https://doi.org/10.1016/j.est.2021.103027.

[23] A.C. Orhan Kalkan, Kadir Bakirci, Ahmet Selim Dalkilie, Experimental investigation of thermal performance of novel cold plate design used in a Li-ion pouch-type battery, Appl. Therm. Eng. 191 (2021).

[24] Y. Zhang, et al., Performance comparison between straight channel cold plate and inclined channel cold plate for thermal management of a prismatic LiFePO4 battery, Energy 248 (2022), https://doi.org/10.1016/j.energy.2022.123637.

[25] G.-H. Kim, K. Smith, K.-J. Lee, S. Santhanagopalan, A. Pesaran, Multi-domain modeling of lithium-ion batteries encompassing multi-physics in varied length scales, J. Electrochem. Soc. 158 (8) (2011), https://doi.org/10.1149/1.3597614.

[26] D.S. Kaushik, High fidelity fast running multi-scale multi physics battery pack software, in: General Motors Global Research and Development, 2018.

[27] K.H. Kwon, C.B. Shin, T.H. Kang, C.-S. Kim, A two-dimensional modeling of a lithium-polymer battery, J. Power Sources 163 (1) (2006) 151–157, https://doi.org/10.1016/j.jpowsour.2006.03.012.

[28] X. Hu, S. Li, H. Peng, A comparative study of equivalent circuit models for Li-ion batteries, J. Power Sources 198 (2012) 359–367, https://doi.org/10.1016/j.jpowsour.2011.10.013.

[29] H. Zhang, C. Li, R. Zhang, Y. Lin, H. Fang, Thermal analysis of a 6s4p Lithium-ion battery pack cooled by cold plates based on a multi-domain modeling framework, Appl. Therm. Eng. 173 (2020), https://doi.org/10.1016/j.applthermaleng.2020.115216.

[30] Batemo Cell library -LG CHEM E66A. https://www.batemo.de/products/batemo-cell-library/e66a/ accessed December 11, 2021.

[31] B. Ye, M. Rubel, H. Li, Design and optimization of cooling plate for battery module of an electric vehicle, Appl. Sci. 9 (4) (2019), https://doi.org/10.3390/app9040754.

[32] U. Desideri, M.A. Perez Estevez, C. Caligiuri, M. Renzi, L. Ferrari, J. Yan, A CFD thermal analysis and validation of a Li-ion pouch cell under different temperatures conditions, E3S Web Conf. 238 (2021), https://doi.org/10.1051/e3sconf/202123809003.

[33] T. Sun, et al., Modeling the inhomogeneous lithium plating in lithium-ion batteries induced by non-uniform temperature distribution, Electrochim. Acta 425 (2022), https://doi.org/10.1016/j.electacta.2022.140701.